RSC Advances

ROYAL SOCIETY OF CHEMISTRY

www.rsc.org/advances

MoS_2/reduced graphene oxide hybrid structure and its tribological property

Mingsuo Zhang, Beibei Chen, Jin Yang, Hongmei Zhang, Qing Zhang, Hua Tang and Changsheng Li*

Abstract: In this study, MoS_2/reduced graphene oxide hybrid material (MoS_2/RGO) was synthesized through a facile and effective hydrothermal method. Fe-Ni matrix composites with different weight fractions of MoS_2/RGO were prepared by powder metallurgy (P/M) technique (1%, 3%, 5%, 7%), and their tribological properties at the temperature ranging from room temperature to 600℃ were investigated using a UMT-2 ball-on-plate friction and wear tester. Results showed that MoS_2 nanospheres composed of many petal-like nanosheets were well attached to the creased RGO sheets. The Fe-Ni matrix composites with suitable MoS_2/RGO content exhibited excellent friction-reducing and anti-wear properties over a wide temperature range, and the RGO in MoS_2/RGO hybrid material played an important role in the hardness and tribological performance of composites. In particular, the specimen with 3 wt% MoS_2/RGO showed the lowest friction coefficient (0.21) and the most stable value of wear rate ($1.07\text{-}1.90\times10^{-5}$ mm^3 N^{-1} m^{-1}). And at 600℃, the friction coefficient was less than 0.30 and the wear rate was 1.07×10^{-5} mm^3 N^{-1} m^{-1} due to the lubricating effect of sulfide films and glaze layer formed on the friction surface at high temperature. The excellent tribological behavior of composites was attributed to the synergetic effect of high hardness and solid lubricants.

Key words. MoS_2/RGO; hybrid structure; Fe-Ni matrix composites; tribological

property; high temperature.

1. Introduction

Metal matrix composites (MMCs) have been widely used in many applications because of high specific modulus, mechanical strength, thermal stability, stable coefficient of friction, and excellent wear resistance compared to pure metals or alloys materials.[1, 2] Currently, nickel matrix composites with high strength, good oxidation resistance and tribological properties at high temperature have been paid increased attention, primarily in advanced engines and gas turbines.[3, 4] The friction coefficients of about 0.2-0.6 were obtained at all the test temperatures.[5-7] Nevertheless, the high cost of nickel matrix composites has restricted their commercial applications significantly. Iron has been considered as a matrix material due to the low cost, abundance and good mechanical properties.[8] Han et al.[9] found that Fe-10Mo-8%CaF_2 had the lowest friction coefficient at room temperature and 600℃. They were 0.38 and 0.23, respectively. Cui et al.[10] investigated the tribological properties of Fe-Cr matrix self-lubricating composites against Si_3N_4 at high temperature. They found that the specimen containing 8.0 wt% BaF_2, 10.0 wt% Ag and 8.5 wt% Mo kept the lowest friction coefficient (0.4) from room temperature to 800℃. Therefore, it will be very significant to develop Fe matrix self-lubricating composites with low friction coefficient and ware rate as the substitute for nikel matrix composites. However, there are few publications on the application of Fe-Ni matrix composites in the tribological field.

As is well known, one of the most effective ways to control friction is to use solid

lubricating materials in the MMCs.[11] So far, various fillers have been attempted to improve the tribological properties of metal matrix,[6, 12, 13] i.e., MoS_2, WS_2, $MoSe_2$, NbS_2, graphite etc. Among them, MoS_2, one of the typical representatives of transition metal sulfide, is the famous known solid lubricant under dry conditions.[14] Its excellent tribological properties are largely attributed to its characteristic layered structures consisting of covalently bound S-Mo-S trilayers and inert basal planes existing in the individual crystallites.[15] However, the majority of the composites developed in the past contain a high percentage of MoS_2 (15-40%) to obtain a low friction coefficient, which would deteriorate mechanical properties of composites.[16] In order to overcome this shortcoming, one method is to add a small amount of MoS_2. So most of MoS_2 are decomposed during sintering, and molybdenum can dissolve into alloy and reinforce the matrix.[6] Another way is to add hard ceramic particles such as SiC, Al_2O_3, WC, TiC and ZrO_2 to produce high strength and wear resistant materials. Zhang et al.[17] have fabricated Fe-28Al-5Cr composites containing TiC, and found that the addition of hard TiC could significantly improve wear resistance of the Fe-28Al-5Cr alloy at high temperatures. Song et al.[18] have studied the wear behavior of WC_P-reinforced iron matrix composites and reported that the wear resistance of which is 1.93 times higher than high-speed steel. Prabhu et al.[19] have investigated the wear properties of Fe/SiC particulate metal matrix composites and found that Fe/SiC composites have excellent abrasive wear resistance.

Graphene, a new crystalline form of carbon with a two-dimensional (2D) platform, has already attracted considerable research interest in many different fields because of

its outstanding properties.[20, 21] Recently, its tribological applications have also been explored due to its extremely high mechanical strength, unique flexible graphitic layers, and easy shear capability on its densely packed and atomically smooth surface,[22, 23] showing great potential to be used as a reinforcing and lubricating phase. For instance, Xu et al.[24] have reported that the presence of multilayer graphene in TiAl matrix composites can greatly improve mechanical properties and decrease friction coefficient and wear rate of composites. Wang et al.[25] have found that graphene had a high fracture strength of 125 GPa, making it an ideal reinforcement phase for in aluminum matrix composites. Tai et al.[26] also reports that the mechanical and tribological properties of graphene oxide (GO)/ultrahigh molecular weight polyethylene (UHMWPE) composites can be improved significantly by adding only a small amount of GO. Based on above discussion, it can be believed that the combination between MoS_2 and graphene will improve the mechanical and tribological properties of composites. However, to the best of our knowledge, there are few efforts devoted to the research of MoS_2/graphene as a filler in the MMCs.

In the study, MoS_2/RGO hybrid material had been successfully synthesized by a facile hydrothermal method. And the as-prepared MoS_2/RGO had been used as a solid filler for Fe-Ni matrix to evaluate its mechanical and tribological properties. Fe-Ni matrix self-lubricating composites containing different MoS_2/RGO contents were prepared through powder metallurgy (P/M) method, in which the addition of Cu powders was further to enhance the strength of composites. The friction and wear properties were studied by ball-on-disc high-temperature tribometer from room

temperature to 600℃. The wear mechanisms were discussed in detail. Hopefully, this study can provide some guidance for designing high-performance Fe-Ni matrix self-lubricant composites.

2. Experimental

2.1. Materials

Graphene oxide (GO) was prepared by exfoliation of graphite according to a modified Hummer method.[27] 0.1 g of GO was then dispersed into 15 ml of deionized water under ultrasonication for 1 h. 1 g Na_2MoO_4, 1.4 g thiourea and 0.5 g PVP were added, following by addition of 5 ml of 0.75 M NaOH solution. The precursor solution was magnetically stirred for 0.5 h. Subsequently, the mixture was then transferred into a 100ml Teflon-lined autoclave for hydrothermal treatment at 200℃ for 24 h. The product was centrifuged, washed and dried in a vacuum oven at 60℃ for 8 h to obtain the MoS_2/RGO hybrid material. For comparison, RGO nanosheets were prepared at the same condition without the addition of Na_2MoO_4 and thiourea. MoS_2 particles were obtained following the same procedure except that no GO were added.

The Fe-Ni matrix self-lubricant composites with different contents of (0, 1, 3, 5, and 7 wt%) MoS_2/RGO were fabricated by a powder metallurgy method. Specially, the powders of iron (76 um), nickel-tungsten-chromium alloy (40 um), copper (50 um) and MoS_2/RGO composites were mechanically mixed, and the components of Fe-Ni matrix composites (denoted as FN, FNRM1, FNRM3, FNRM5 and FNRM7) were listed in Table 1. The composites powders were then cold-pressed at 150 MPa and sintered pressurelessly in argon gas at 1100℃ for 1h. For comparison, Fe-Ni matrix

composites with different solid lubricant additions (3 wt% RGO and 3 wt% MoS_2) were prepared by the same procedure.

Table 1 Composition of Fe -Ni matrix self-lubricant composites

Specimens	Fe (wt%)	Ni-W-Cr alloy powder (wt%)	Cu (wt%)	MoS_2/RGO (wt%)
FN	60	30	10	0
FNRM1	59	30	10	1
FNRM3	57	30	10	3
FNRM5	55	30	10	5
FNRM7	53	30	10	7

2.2. Characterization

The morphologies and microstructures of the as-prepared MoS_2/RGO hybrid material were characterized by scanning electron microscopy (SEM, JSM-7001F, JEOL) and transmission electron microscopy (TEM, JEM-2100, JEOL). XRD measurement with a D8ADVANCE X-ray diffractometer (Bruker Corporation, Germany) and Cu Kα targets in the 2θ range of 5-80° (λ = 0.1546 nm) was used for phase analysis. X-ray photoelectron spectroscopy (XPS) measurements were performed on an ultrahigh vacuum VG ESCALAB 250XI electron spectrometer. Raman spectra was performed on the GO and MoS_2/RGO using a Renishaw inVia spectrometer with an excitation laser of 532 nm in wavelength.

The sintered density of composites was determined by the Archimedes' method. The Vickers hardness was measured by using an MH-5 Vickers hardness instrument (Shang Hai Heng Yi Technology Company, China). The test load is 300 g and a dwell time is 10 s. For each sample, ten tests were conducted and the mean value was shown in Table 2.

The friction and wear tests were carried out on a universal micro-tribotester with a ball-on-disc contact configuration (UMT-2, Center for Tribology Inc, USA). The disks, which were the as-prepared materials, were cleaned with acetone and then dried in hot air before test. The commercial alumina ceramic ball with a diameter of 9 mm (about HRC70) was used as the counterpart. The selected test temperatures were room temperature, 200, 400 and 600℃. The friction experiment was measured at a sliding speed of 0.08 m/s and load of 10 N for 15 min. The profile of the worn surface cross-section was measured using a SURFCOM 130A roughmeter and the wear volume was calculated as $V=AL$, where A was the cross-section area of worn scar in mm^2, and for each wear track four locations were measured to determine the value of the cross-sectional area A, and L was the length of the worn scar in mm. Then, the wear rate, $W=V/SF$, was calculated as wear volume divided by sliding distance S in meter and the applied load F in Newton. The morphology and structure of specimen FNRM3 were analyzed by SEM and XRD and worn surfaces were observed using SEM. All the tribological tests were carried out at least three times to make sure the reproducibility of the experimental data under the same condition.

3. Results and discussion

3.1. Microstructure of MoS_2/RGO hybrid material

Fig.1 shows a comparison of the XRD patterns of as-prepared RGO, MoS_2 and MoS_2/RGO. RGO has two broad peaks at about $2\theta = 23°$ and 43°, which are related to the (002) inter-planar spacing of 0.4 nm and (100) that of 0.2 nm, respectively.[28] The (002) crystal plane is very broad, suggesting that the sample is very disorderedly

along the stacking direction. All observed diffraction peaks related to MoS_2 have been indexed to the hexagonal MoS_2 phase (JCPDS No. 37-1492) with lattice constants a = 3.161 Å, b = 3.161 Å, c = 12.84 Å. No other peaks from impurities are observed in the XRD pattern, indicating that the sample was highly pure. In addition, it can also be observed that the MoS_2/RGO hybrid material basically retain the layered crystallinity and the position of the diffraction peaks of MoS_2. However, it is worth noticing that the intensity of all the diffraction peaks of MoS_2 decrease with the addition of RGO, which indicates that the incorporation of the RGO considerably inhibits the growth of MoS_2 crystals. Additionally, the diffraction peaks of the RGO nanosheets could hardly be detected in the MoS_2/RGO hybrid material, suggesting of less agglomeration for RGO nanosheets in hybrid material.

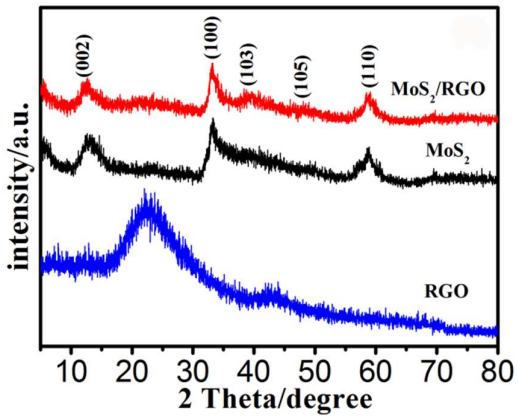

Fig.1 (a) XRD patterns of RGO, MoS_2, MoS_2/RGO.

Fig.2 presents XPS spectra of MoS_2/RGO hybrid material. The Mo 3d peaks (Fig.2a) exhibit a unique doublet at 232.5 and 229.3 eV, respectively, which are typical values for Mo^{4+} in MoS_2. While the S 2p doublet peaks (Fig.2b) at 162.1 and 163.3 eV suggest the existence of S^{2-} in MoS_2.[29] In addition, the Mo/S atomic ratio is determined to be 1:1.94 (~1:2), in good agreement with the nominal atomic

composition of MoS_2.

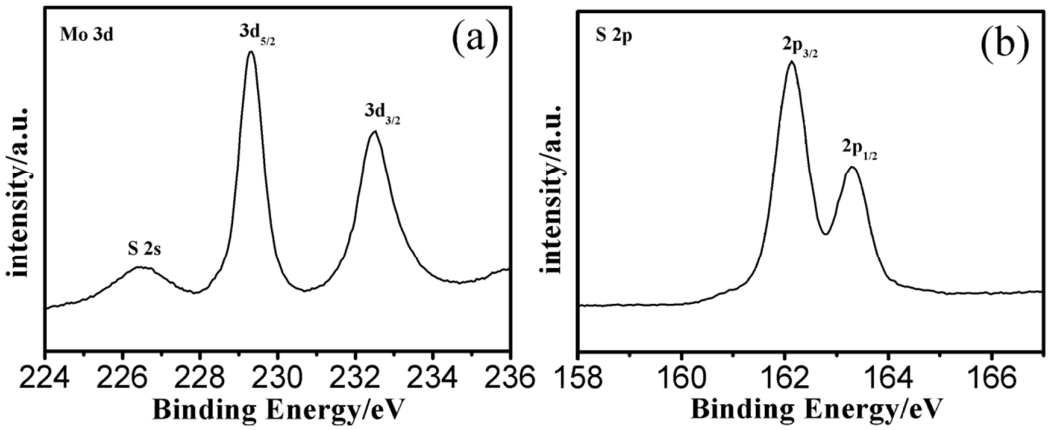

Fig.2 XPS spectra of the Mo 3d and S 2p regions for MoS_2/RGO hybrid material.

Fig.3 shows the Raman spectra of pristine GO and the MoS_2/RGO hybrid material, respectively. The Raman spectra of GO shows two peaks at 1361 cm^{-1} and 1585 cm^{-1}, which correspond to sp^3 (D band) and sp^2 (G band) hybridization carbon atoms, respectively.[30] In comparison to the pristine GO, the Raman spectra of the MoS_2/RGO hybrid material shows that the D and G band shifted to lower wave numbers at 1355 cm^{-1} and 1584 cm^{-1}, respectively. This is because of the effective reduction of GO during the hydrothermal process.[31, 32] Moreover, the D/G intensity ratio of MoS_2/RGO increases compared to that of GO after reduction (from 0.94 to 1.17), suggesting the reduction process leads to the increase of disorder and defects of the RGO layers. Based on the XRD, XPS and Raman spectroscopy results, we confirm that the MoS_2/RGO hybrid material is composed of RGO and MoS_2.

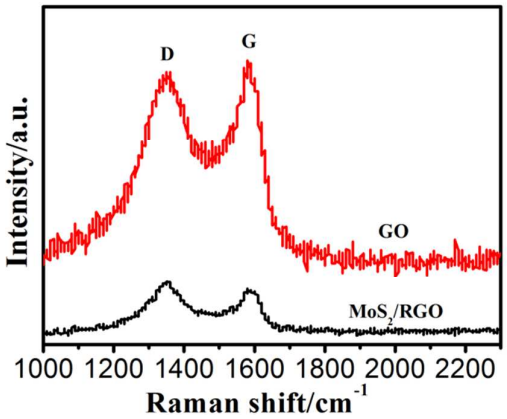

Fig.3 Raman spectra of pristine GO and MoS_2/RGO hybrid material.

Fig.4 shows SEM and TEM images of the as-prepared MoS_2 and MoS_2/RGO. As shown in Fig.4a and b, the obtained MoS_2 particles are spherical and with an average particle size of 450 nm. And the surface of MoS_2 nanosphere is uneven. Fig.4c shows the morphology of the MoS_2/RGO hybrid material. The MoS_2 nanoparticles with the average diameter of 150 nm are well dispersed and attached to the creased RGO sheets. At a higher magnification in Fig.4d, it can be clearly observed that the as-prepared MoS_2 nanospheres consist of many MoS_2 nanosheets. Comparing with pure MoS_2, it is found that the average particle size of MoS_2 particles in MoS_2/RGO hybrid material not only decreases obviously but also the corresponding morphology changes. Ths is because the incorporation of the RGO prevents the growth of the layered MoS_2 crystals during the hydrothermal process, which lead to the poor crystallinity of MoS_2 in MoS_2/RGO hybrid material. These SEM images are in good agreement with the XRD results given in Fig.1a. The TEM image (Fig.4e) shows that most of the MoS_2 nanoparticles lay flat on the RGO nanosheets and the aggregation of MoS_2 was well prevented by the RGO nanosheets. From the inset TEM image in Fig.4e, it is found that MoS_2 nanocrystals are formed from several petal-like MoS_2

nanosheets grown along radial direction through a self-assembly process. In this study, we believe that the growing process of MoS_2 nanospheres is consistent with previous report.[33] More details for MoS_2 structure are illustrated in Fig.4f. It shows that the MoS_2 nanoparticles have a layered structure with interlayer spacings of ca. 0.62, which corresponds to the (002) plane of hexagonal MoS_2 structure.[34]

3.2. Materials features

XRD patterns of the as-prepared FN, FNRM1, FNRM3, FNRM5 and FNRM7 are presented in Fig.5. It can be found that the diffraction peaks primarily belong to the Ni-Solid Solution and FeNi phases in all samples. Moreover, the intensity of Ni-Solid Solution peaks gradually increases and that of FeNi, Fe, Fe-Cr peaks decreases with the increasing MoS_2/RGO contents, and Cr_xS_{x+1} can be found in FNRM composites (FNRMs). This is because most MoS_2 decomposed during pressureless sintering and transformed into Cr_xS_{x+1}.[6] Although MoS_2 reacts with matrix, new phases Cr_xS_{x+1} formed through reaction were also excellent solid lubricants.[35] In addition, the formation of Fe_3W_3C can significantly improve the strength, hardness and wear resistance of composites.[1]

Fig.6a shows the morphology of the specimen FNRM3. It can be observed that the microstructure is dense and homogeneous and there are some obvious deep gray (Area A) and black (Area B) phases. The elements of area marked with A in Fig.6a are mainly comprised of chromium and sulfur (Fig.6b), which is in accordance with Cr_xS_{1+x} in the XRD results of Fig. 5. The Raman spectra (Fig.6c) of area marked with B in Fig.6a presents two main characteristic peaks of graphene: the D and G mode,[24]

which are similar to the Raman spectrum of MoS_2/RGO determined in Fig.3. Consequently, it can be concluded that RGO is retained in the FNRM3 after pressureless sintering.

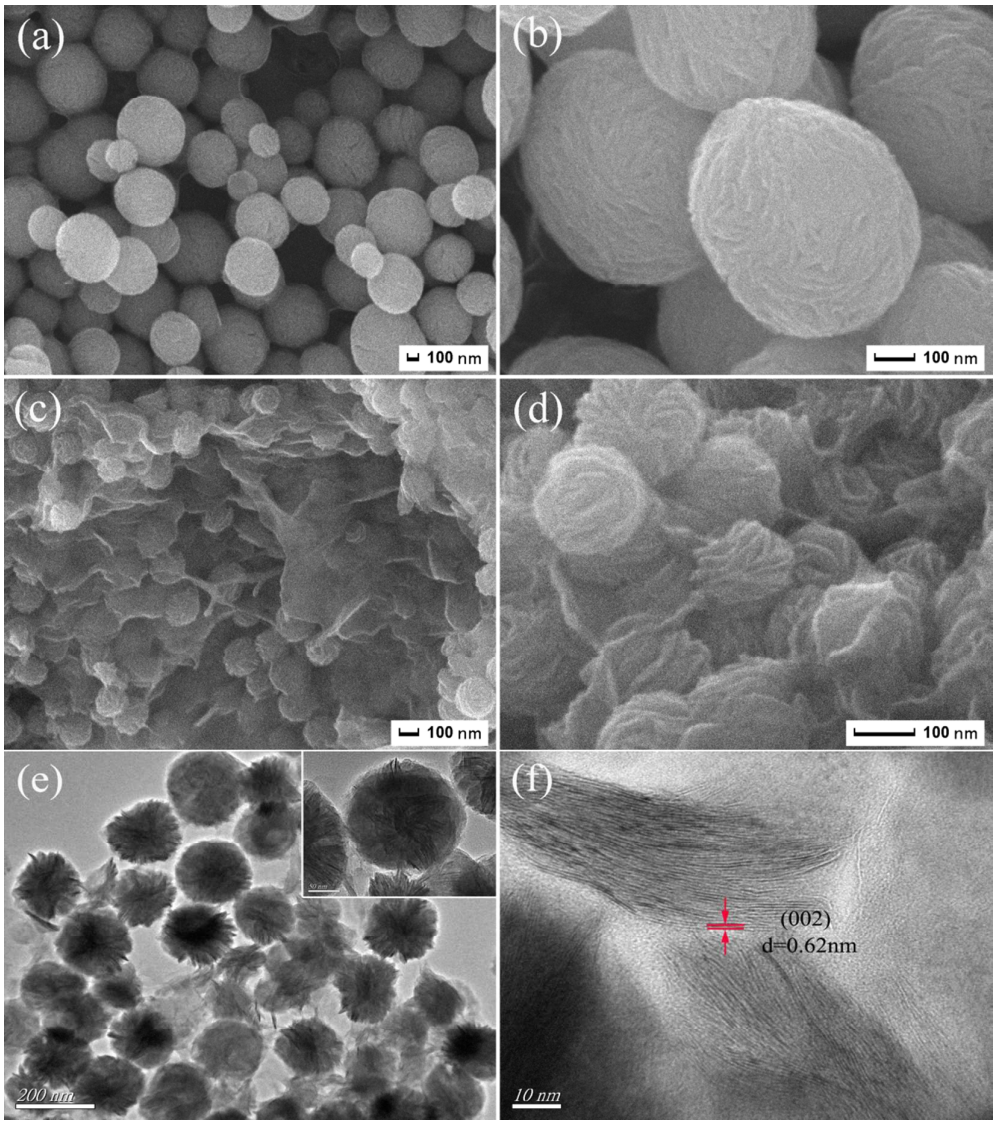

Fig.4 SEM images of MoS_2 particles (a, b) and MoS_2/RGO hybrid material (c, d); (e, f) TEM images of MoS_2/RGO hybrid material.

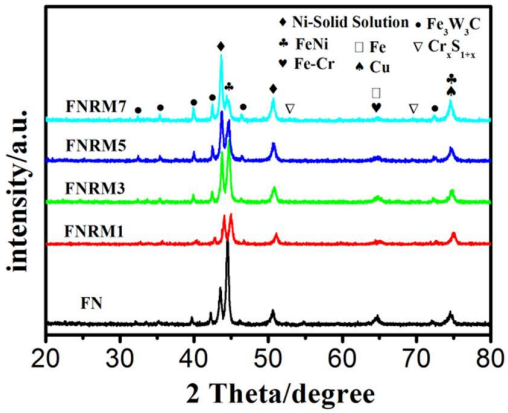

Fig.5 XRD patterns of sintered FN, FNRM1, FNRM3, FNRM5 and FNRM7.

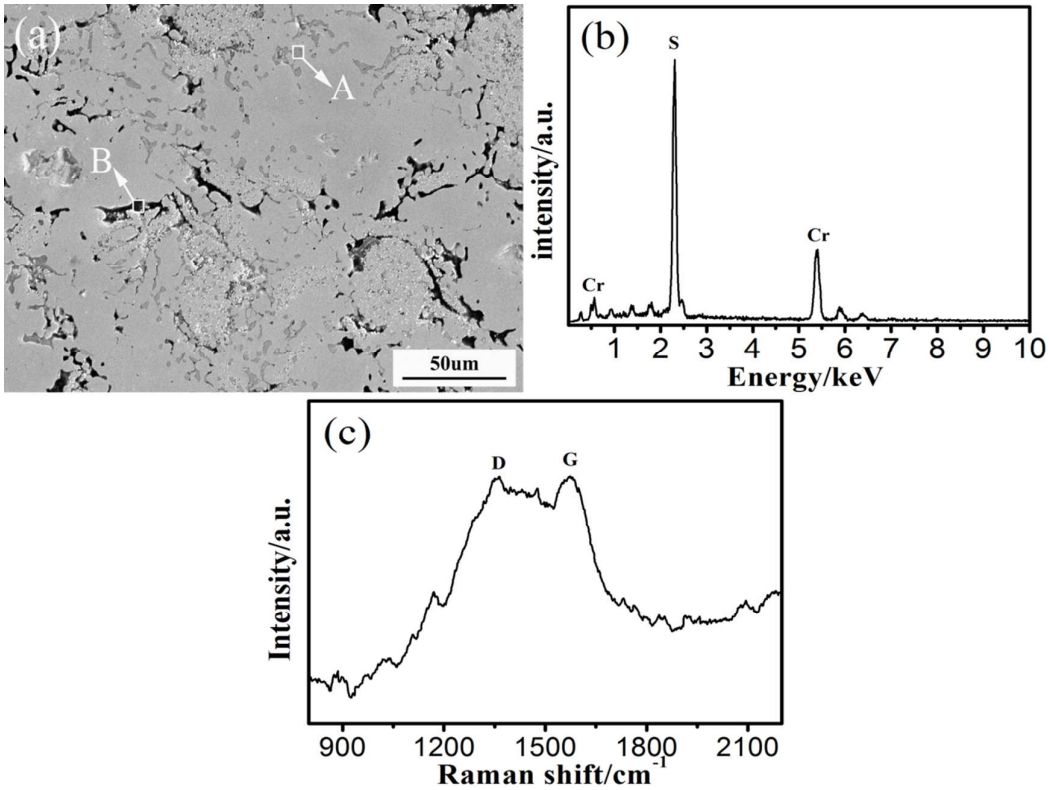

Fig.6 (a) SEM morphology of FNRM3; (b) element of phase A by EDS; (c) Raman spectra of phase B.

Table 2 shows the Vickers hardness and density of Fe-Ni matrix self-lubricant composites. It can been seen that the addition of RGO (specimen FNR) could obviously improve the hardness of Fe-Ni matrix. After adding 1% MoS_2/RGO, the hardness of Fe-Ni matrix composites is higher than that of specimens FNR and FN.

Moreover, with increasing MoS_2/RGO content, the hardness and density of composites are kept at a relatively high value, compared with specimen FN. This is mainly because MoS_2 was decomposed during the sintering process and reacted with metal matrix, molybdenum dissolved into Fe-based alloy and reinforced the Fe-Ni matrix.[6]

Table 2 Vickers hardness and measured density of Fe-Ni matrix self-lubricant composites

	FN	**FNR**	**FNRM1**	**FNRM3**	**FNRM5**	**FNRM7**
Vickers hardness(HV)	130.6	137.2	139.8	138.1	135.8	128.9
Measured density(g/cm^3)	6.271	5.905	6.273	6.359	6.263	6.196

3.3. Friction and wear properties

Fig.7 shows the variation of friction coefficients of composites with sliding time at room temperature and 600℃, respectively. As it is shown in Fig.7, at room temperature and 600℃, the friction coefficients of FNRM3 (3 wt% MoS_2/RGO) composite are much lower than those of FN (0 wt% Additive). And the average friction coefficient decreases by 44% at room temperature and 26% at 600℃. In addition, it is also found that the friction coefficients of dual-lubricant composites (3 wt% MoS_2/RGO) are lower and fluctuate more slightly than those of the single-lubricant composites (3 wt% RGO and 3 wt% MoS_2) at room temperature and 600℃, respectively.

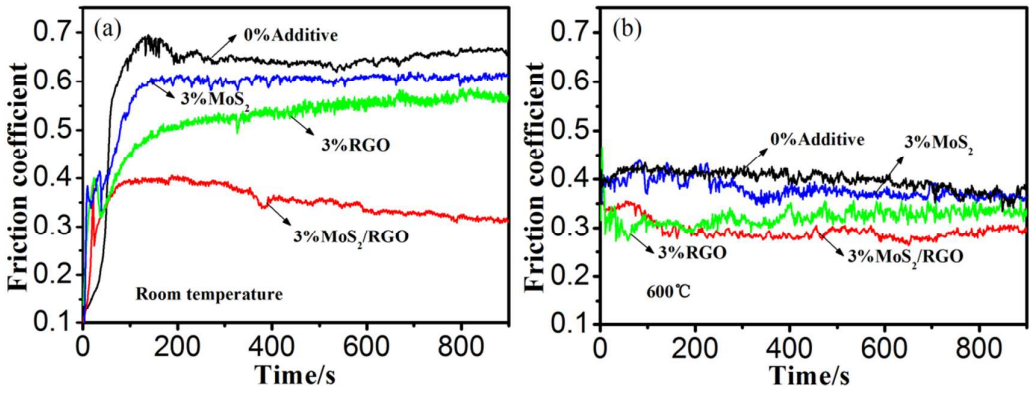

Fig.7 Variations of friction coefficients of different solid lubricants at (a) room temperature and (b) 600℃

The variations of friction coefficients of FN and FNRMs with temperatures are given in Fig.8. It can be found that the friction coefficients of FN sharply decrease with the temperature increasing from room temperature to 400℃, then increase slightly from 400 to 600℃. Compared to specimen FN, FNRM3 and FNRM5 exhibit lower friction coefficients and similar trend over a wide temperature range. Moreover, it can be found that the friction coefficients of FNRM3 (0.21-0.35) are lower than all the other samples at each testing temperature. However, the friction coefficients of FNRM1 and FNRM7 show obvious variation trend with the increase in temperature. It seems that the friction coefficients initially decrease from room temperature to 200℃, and then increase at 200-600℃. Moreover, the friction coefficients of FNRM1 and FNRM7 are clearly higher than that of FN at 400 and 600℃, indicating that too low or too high amounts of MoS_2/RGO is not conducive to improving the self-lubricating performance of Fe-Ni matrix composites at high temperature.

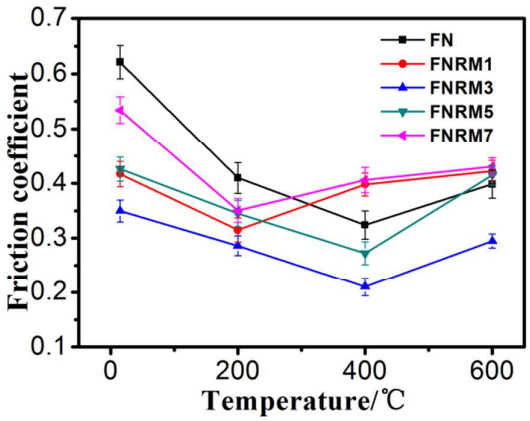

Fig.8 Variations of friction coefficient of specimens FN, FNRM1, FNRM3, FNRM5 and FNRM7 at different testing temperatures.

Fig.9 shows the variations of the wear rate of composites with the elevated temperature at the sliding speed of 0.08 m/s and applied load of 10 N. It can be found that the wear rates of all specimens increase slightly at the temperature below 200℃, and then decrease significantly with the increasing temperature. The wear rates of FN maintain at high level (1.53-3.52×10^{-5} mm^3 N^{-1} m^{-1}) from room temperature to 600℃. After adding MoS_2/RGO, the wear rates of FNRMs are much lower than that of FN over a wide temperature range. Moreover, it could be found that the wear rates of FNRM3 have the most stable value and are below 1.90×10^{-5} mm^3 N^{-1} m^{-1} at all the tested temperatures. FNRM3 exhibits the best tribological performance among all the samples over the temperature range of room temperature-600℃.

Fig.10 shows a SEM-EDS analysis of worn surfaces of FNRM3 composite after tests at different temperatures. It can be noted that the ploughing and flaking pits are on the worn surfaces at room temperature (Fig.10a). At 200℃ (Fig.10b), the worn surface shows slight ploughing and delamination, and the worn surface damage is relatively mild compared with that at room temperature. As temperature increases to

400℃ (Fig.10c), the worn surface is very smooth and a continuous lubrication film is formed, but only slight delamination, which accounts for the lowered friction coefficient and wear rate. However, at 600℃ (Fig.10d), it is characterized by the discontinuous glaze layer covering on the worn surface together some slight delamination. The formation of the discontinuous glaze layer could play an important role in friction reducing and anti-wear properties at high temperature. [12] Thus, the dominant wear mechanism is ploughing and flaking pits at temperatures below 400℃ as well as delamination at 400-600℃. Fig.10e shows the EDS analysis of the worn surface of FNRM3 at 600℃ (Fig.10d). It can be found that the glaze layer contains elements of sulfur, oxygen and alloy elements of Fe, Ni, Cr, W, Cu, Mo. The oxides and sulfide coexist in the glaze layer, which are responsible for friction reduction.

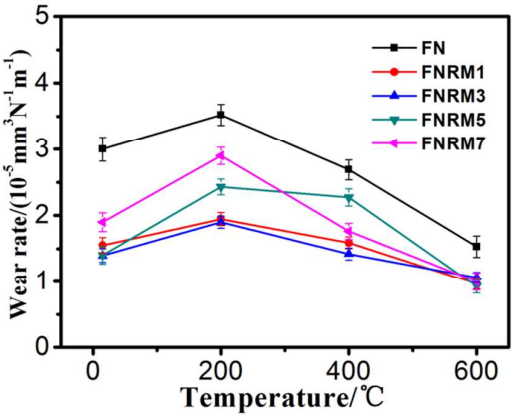

Fig.9 Variations of wear rate of specimens FN, FNRM1, FNRM3, FNRM5 and FNRM7 at different testing temperatures.

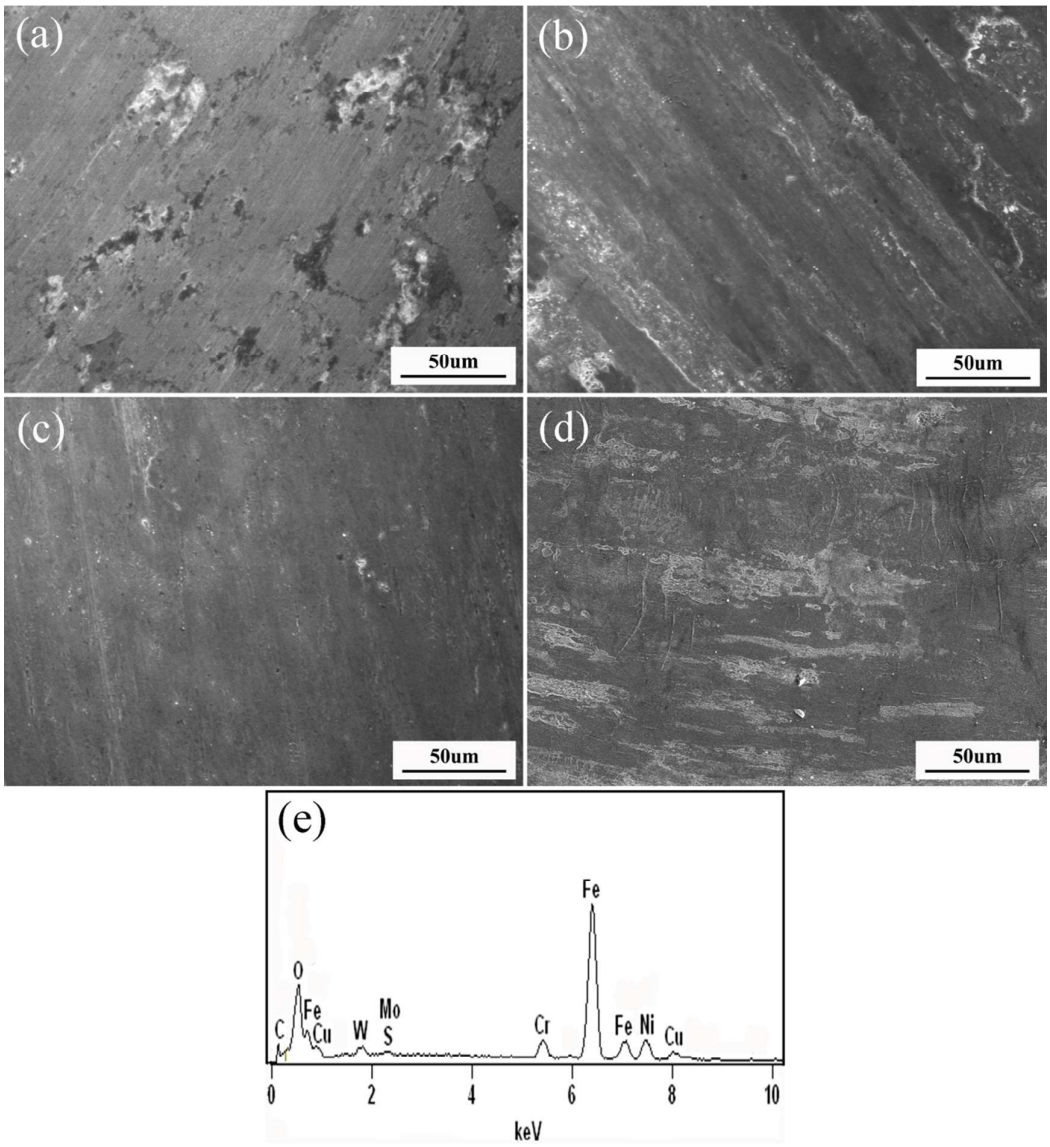

Fig.10 SEM micrographs of worn surface of specimen FNRM3: (a) room temperature, (b) 200℃, (c) 400℃ and (d) 600℃; (e) EDS analysis of (d).

Fig.11 compares the EDS analysis results of the worn surfaces of FNRMs at 600℃. In the case of FNRM1 (Fig.11a), the concentration of sulfur on the friction surface is poor, which is not enough to form a lubrication film. When the MoS_2/RGO content increases to 5 wt% (Fig.11b) and 7 wt% (Fig.11c), sulfur content has been a little higher. According to the previous reports,[36] after the sulfide in the nickel alloy come into being eutectic and their melting point decreased to 600-900℃ from 1300℃.

Low-melting-point eutectic sulfides are partly melted by the action of high contacting temperature on the friction surface. Meanwhile, the high-valance chromium sulfide in the eutectic sulfide would decompose and be oxidized due to thermal effect, and gradually changed into low-valance chromium sulfide.[6] Comparing with specimen FNRM3, more sulfide content is exposed to air at 600℃ in specimens FNRM5 and FNRM7, which may cause that the melting or intenerating rate is lower than the decomposing rate. The concentration of sulfur on the friction surface decreases and the synthesis compound Cr_2O_3 with high hardness at elevated temperature will damage the lubrication film as abrasive particle. Finally, the lubricating effect of sulfide is weaken. Therefore, the optimum adding amount of MoS_2/RGO is 3 wt%.

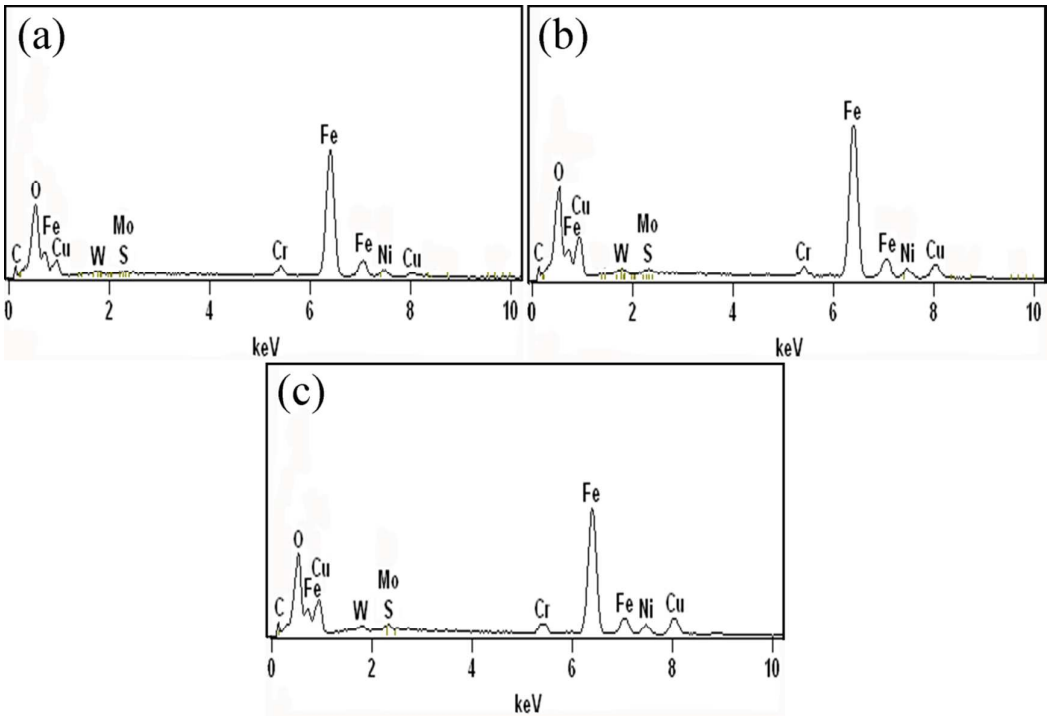

Fig.11 EDS analysis of the worn surfaces of specimens (a) FNRM1, (b) FNRM5 and (c) FNRM7 at 600℃.

4. Conclusions

(1) A facile and effective hydrothermal method was developed to synthesize MoS_2/RGO hybrid material. And the size of MoS_2 nanospheres composed of many petal-like nanosheets was about 150 nm.

(2) Fe-Ni matrix self-lubricating composites with MoS_2/RGO were prepared by powder metallurgy (P/M) method. The composites were mainly consisted of Ni-Solid Solution, FeNi, Fe_3W_3C, Cr_xS_{x+1} and RGO. The Vickers hardness and density of composites can be increased by adding suitable amount of MoS_2/RGO.

(3) The composites with MoS_2/RGO possess more excellent friction and wear properties due to the combined effects of solid lubricants and high hardness than specimen FN over a wide range of temperature. The optimum MoS_2/RGO amount for tribological properties is 3 wt%. The friction coefficients of 0.21-0.35 are obtained and the wear rate is $1.07\text{-}1.90\times10^{-5}$ mm^3 N^{-1} m^{-1} from room temperature to 600℃.

(4) The dominant wear mechanism for FNRM3 is ploughing and flaking pits below 200℃ as well as delamination at 400 and 600℃.

Acknowledgements

This research was financially supported by the National Nature Science Foundation of China (Grant No. 51405199, 51275213, 51302112), Natural Science Foundation of Jiangsu Province (Grant No. BK20140551 and BK20140562), the Jiangsu Industry-University-Research Jointinnovation Foundation (BY213065-05, BY213065-06) and a Project Funded by Priority Academic Program Development of Jiangsu Higher Education Institutions.

Notes and references

School of Materials Science and Engineering, Jiangsu University, Key Laboratory of high-end structural materials of Jiangsu Province, Zhenjiang, Jiangsu 212013, P.R. China. Fax: +86 511 8879 0268; Phone: +86 511 8879 0268; E-mail: lichangsheng@mail.ujs.edu.cn

[1] K. H. Zheng, Y. M. Gao, S. L. Tang, Y. F. Li, S. Q. Ma, D. W. Yi and Z. Y. Zhang, *Tribol. Lett.*, 2014, **54**, 15.

[2] Y. Zhan and G. Zhang, *Mater. Design*, 2006, **27**, 79.

[3] X. F. Lu and H. M. Wang, *J. Alloys Comp.*, 2009, **469**, 472.

[4] N. L. Parthasarathi and M. Duraiselvam, *J. Alloys Comp.*, 2010, **505**, 824.

[5] R. Tyagi, D. S. Xiong, J. L. Li and J. H. Dai, *Wear*, 2010, **269**, 884.

[6] J. L. Li, D. S. Xiong and M. F. Huo, *Wear*, 2008, **265**, 566.

[7] E. Y. Liu, Y. M. Gao, W. Z. Wang, X. L. Zhang, X. Wang, G. W. Yi and J. H. Jia, *Tribol. Lett.*, 2012, **47**, 399.

[8] A. Kelly, *J. Mater. Sci.*, 2006, **41**, 905.

[9] J. S. Han, J. H. Jia, J. J. Lu and J. B. Wang, *Tribol. Lett.*, 2009, **34**, 193.

[10] G. J. Cui, L. Lu, J. Wu, Y. P. Liu and G. J. Gao, *J. Alloys Comp.*, 2014, **611**, 235.

[11] D. Berman, A. Erdemir and A. V. Sumant, *Mater. Today.*, 2014, **17**, 31.

[12] M. Y. Niu, Q. L. Bi, S. Y. Zhu, J. Yang and W. M. Liu, *J. Alloys Comp.*, 2013, **555**, 367.

[13] Y. Z. Zhan and G. D. Zhang, *Tribol. Lett.*, 2004, **17**, 91.

[14] J. S. Zabinski and M. S. Donley, *Thin Solid Films*, 1992, **214**, 156.

[15] C. Donnet and A. Erdemir, *Tribol. Lett.*, 2004, **17**, 389.

[16] X. L. Shi, S. Y. Song, W. Z. Zhai, M. Wang, Z. Xu, J. Yao, A. Q. Din and Q. X. Zhang, *Mater. Design*, 2014, **55**, 75.

[17] X. H. Zhang, J. Q. Ma, L. C. Fu, S. Y. Zhu, F. Li, J. Yang and W. M. Liu, *Tribol. Int.*, 2013, **61**, 48.

[18] Y. P. Song, H. Yu, J. G. He and H. G. Wang, *J. Mater. Sci.*, 2008, **43**, 7115.

[19] T. R. Prabhu, V. K. Varma and S. Vedantam, *Wear*, 2014, **309**, 1.

[20] A. K. Geim and K. S. Novoselov, *Nat. Mater.*, 2007, **6**, 183.

[21] H. P. Li, L. Chen, Y. Zhang, X. R Ji, S. Chen, H. J. Song, C. S. Li and H. Tang, *Cryst. Res. Tech.*, 2014, **49**, 204.

[22] D. Berman, A. Erdemir and A.V. Sumant, *Carbon*, 2013, **54**, 454.

[23] M. S. Zhang, B. B. Chen, H. Tang, G. G. Tang, C. S. Li, L. Chen, H. M. Zhang and Q. Zhang, *RSC Adv.*, 2015, **5**, 1417.

[24] Z. S. Xu, X. L. Shi, W. Z. Zhai, J. Yao, S. Y. Song and Q. X. Zhang, *Carbon*, 2014, **67**, 168.

[25] J. Y. Wang, Z. Q. Li, G. L. Fan, H. H. Pan, Z. X. Chen and D. Zhang, *Scr Mater*, 2012, **66**, 594.

[26] Z. X. Tai, Y. F. Chen, Y. F. An, X. B. Yan and Q. J. Xue, *Tribol. Lett.*, 2012, **46**, 55.

[27] W. S. Hummers and R. E. Offeman, *J. Am. Chem. Soc.*, 1958, **80**, 1339.

[28] C. Wang, C. Feng, Y. J. Gao, X. X. Ma, Q. H. Wu and Z. Wang, *Chem. Eng. J.*,

2011, **173**, 92.

[29] Y. X. Li, H. Wang and S. Q. Peng, *J. Phys. Chem. C*, 2014, **118**, 19842.

[30] T. Kamegawa, D. Yamahana and H. Yamashita, *J. Phys. Chem. C*, 2010, **114**, 15049.

[31] Q. J. Xiang, J. G. Yu and M. Jaroniec, *Nanoscale*, 2011, **3**, 3670.

[32] X. Y. Zhang, H. P. Li, X. L. Cui and Y. H. Lin, *J. Mater. Chem.*, 2010, **20**, 2801.

[33] G. G. Tang, J. R. Sun, W. Chen, H. Tang, Y. Wang and C. S. Li, *Mater. Lett.*, 2013, **100**, 15.

[34] K. Chang, W. X. Chen, L. Ma, H. Li, H. Li, F. H. Huang, Z. D. Xu, Q. B. Zhang and J. Y. Lee, *J. Mater. Chem.*, 2011, **21**, 6251.

[35] C. Y. Kan, J. Z. Liu, G. W. Zhang and J. L. Ouyang, *Tribology*, 1994, **14**, 193 (In Chinese).

[36] R. T. Liu, X. B. Li, D. S. Xiong and S. H. Cheng, *J. Cent. South Univ. Technol.*, 2000, **31**, 260 (In Chinese).